

Rapid high-temperature metamorphism of East Pacific Rise gabbros from Hess Deep

Craig E. Manning^{*}, Patricia E. Weston, Keith I. Mahon

Department of Earth and Space Sciences, University of California at Los Angeles, Los Angeles, CA 90024-1567, USA

Received 22 February 1996; revised 24 June 1996; accepted 29 July 1996

Abstract

Metamorphosed oceanic gabbros provide a record of the cooling history of the lower crust near mid-ocean ridges, but the temperature range, rate, and location of subsolidus events are poorly known. We combine hornblende–plagioclase thermometry, statistical analysis, and thermal models to estimate precisely the temperature, time, distance from axis, and duration of metamorphism in East Pacific Rise gabbros from Hess Deep, ODP Hole 894G. Metamorphic hornblende and plagioclase, which formed during microfracturing and sea water penetration, equilibrated at a mean temperature of $716 \pm 8^\circ\text{C}$ (90% confidence level). Comparison of the properties of the observed temperature distribution with those of model events indicates that metamorphism spanned $\leq 60^\circ\text{C}$. When combined with thermal models of fast-spreading centers, this implies that metamorphism was rapid (≤ 6000 yr) and occurred 1–4 km off axis. Application of this approach to other gabbros will allow comparison of spatial and temporal characteristics of deformation and fluid flow in the lower oceanic crust as a function of ridge setting.

Keywords: East Pacific Rise; ODP Site 894; hydrothermal processes; metamorphic rocks; amphibolite facies; metagabbro; metaplutonic rocks; geologic thermometry; P-T conditions; microcracks

1. Introduction

The time, location, and duration of deformation and fluid flow drive metamorphism in oceanic gabbros controls the lower crust's contribution to heat and mass transfer in the oceanic lithosphere. Determination of the temporal characteristics of subsolidus events in the lower crust (i.e., its thermal history) is therefore an important goal for studies of oceanic gabbro metamorphism. However, although

the compositions and textures of metamorphic minerals in the gabbros provide a record of subsolidus events, this record lacks the precision necessary to provide a clear view of whether metamorphism spans broad or narrow temperature intervals, whether it is rapid or slow, or where it occurs relative to ridge axes.

Metamorphism of oceanic gabbros usually begins at high grades, regardless of spreading rate or style of deformation [1,2]. The typical early mineral assemblage of hornblende + plagioclase + Fe–Ti oxide \pm clinopyroxene implies temperatures of between ~ 500 and $\sim 800^\circ\text{C}$ at the pressures and oxygen

^{*} Corresponding author. Tel.: +1 310 206 3290. Fax: +1 310 825 2779. E-mail: manning@ess.ucla.edu

fugacities of the oceanic lower crust [3,4]. This limit is too broad to help discern where metamorphism occurs within this interval. Mineral thermometers can potentially circumvent this problem. For example, where present, metamorphic clinopyroxenes can be combined with the well calibrated geometry of the pyroxene solvus [5] to place limits on temperatures of gabbro metamorphism [6,7]. However, temperature estimates are typically no better than those given by the mineral assemblage itself [2,8] and, in the absence of well characterized error estimates and statistical analysis of the temperature distribution, such thermometry-based results provide few additional constraints on thermal history.

In this paper we show that the temperature and timing of early metamorphism of oceanic gabbros can be determined more precisely. Using metamorphosed gabbros of the East Pacific Rise (EPR) from Hess Deep, we combine plagioclase–hornblende exchange thermometry [9] with a simple statistical analysis of metamorphism and thermal models to derive the location, timing, and duration of pervasive metamorphism of lower crust near the East Pacific Rise. Our results show that, to a high level of confidence, metamorphism occurred at high temperatures, and over a narrower temperature range and shorter duration than has previously been recognized.

2. Metamorphism of Hess Deep gabbros

Hess Deep (101°30'W, 2°15'N) is a submarine rift valley in ~1 m.y. old EPR crust at the western terminus of the Cocos–Nazca spreading center ~50–100 km east of the present spreading axis [10,11]. Stratigraphically continuous ultramafic rocks, gabbroic rocks, sheeted dikes, and pillow lavas exposed in the valley walls record EPR crustal processes at a half spreading rate of 65 mm/yr [11]. Ocean Drilling Program Hole 894G penetrated 154.5 m of poikilitic to equigranular gabbro, gabbro norite, and olivine gabbro norite [12], all of which we refer to as gabbros. The gabbros crystallized 2–3 km below sea floor, immediately beneath the typical stratigraphic position of the axial magma lens [13].

The earliest gabbro metamorphism is recorded as a microfracture network filled by calcic amphibole and related, pervasive alteration of the gabbros to

amphibolite-facies mineral assemblages [14]. Progressively later vein types are macroscopic amphibole veins, chlorite-bearing veins, and zeolite–calcite veins. The veins record discrete fracturing events during the progressive decline in temperature as the gabbros moved off the EPR. Based on orientations and timing, Manning and MacLeod [14] inferred that microscopic and macroscopic amphibole veins record deformation and metamorphism associated with near-ridge fracturing, faulting, and hydrothermal activity, whereas chlorite-bearing and zeolite–calcite veins record deformation and fluid flow during interaction with the Cocos–Nazca spreading center.

The focus of our investigation was on the early microscopic amphibole veins because they constrain the timing and temperature of the earliest and most extensive brittle failure, fluid flow, and metamorphism in the lower crust near the East Pacific Rise [14]. The microfractures are $\leq 40 \mu\text{m}$ wide; they are filled by green, blue-green, and olive-green calcic amphibole; and they occur along grain boundaries and cutting magmatic mineral grains. Microscopic amphibole veins are pervasive in the core and are responsible for the largest fraction of metamorphic minerals (10% to >50%) [12,14].

Alteration of magmatic minerals at the margins of microscopic amphibole veins varies depending on the mineral hosting the vein [14]. Magmatic clinopyroxene is typically partially to completely replaced by calcic amphibole and minor secondary clinopyroxene (Fig. 1). Optically, plagioclase appears unaffected by amphibole alteration; however, back-scattered electron petrography reveals a pervasive, abrupt change in average atomic number in plagioclase rims near microscopic amphibole veins and related replacement features (Fig. 1). Usually this is compositionally subtle, reflecting a decrease in An content of 10% or less; but in rare cases the An content decreases dramatically. These compositional shifts are spatially correlated with amphibole veins and are therefore interpreted as metamorphic in origin, as distinct from the typical optically observable magmatic growth zoning, which is related to crystal morphology [15]. Subordinate orthopyroxene, olivine, and Fe–Ti oxide are altered to intergrowths of cumingtonite–actinolite, actinolite–talc, and magnetite–ilmenite, respectively. Alteration in several decimeter scale pegmatitic gabbros is more pervasive

and more complex, in that amphibole and plagioclase are strongly zoned. Metamorphism of pegmatites may have begun during the latest stages of crystal-

lization, possibly associated with magmatic fluids [16], and preliminary studies of phase equilibria also suggest longer metamorphic duration [17]. Because

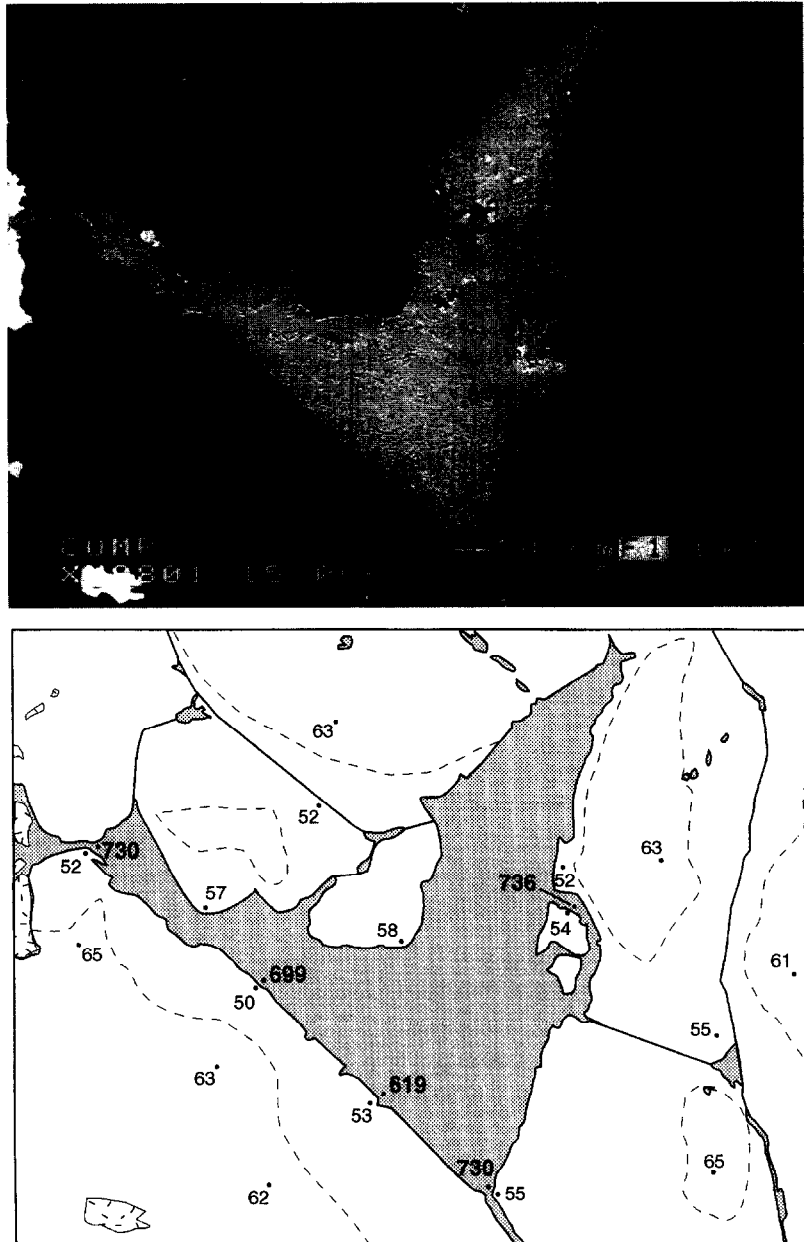


Fig. 1. Backscattered electron photomicrograph and tracing of microscopic amphibole veins and replaced clinopyroxene in sample 4R-02-7 (48.2 m below sea floor). Bold lines = grain boundaries; blank areas = plagioclase (dashed lines separate compositionally distinct zones); light shading = amphibole and minor magnetite; random dashes = holes in C coat. Dots show positions of hornblende and plagioclase analyses; plagioclase analyses labeled with X_{An} , amphibole analyses with calculated temperature using adjacent plagioclase composition.

their metamorphic history appears to be different from that of nonpegmatitic gabbros, pegmatitic samples were excluded from this analysis.

3. Mineral compositions

We selected nine gabbro samples for detailed study. The samples represent the range in depth, grain size, and magmatic mineral modes in Hole 894G; all are petrographically unaffected by the later alteration events described above. Compositions of 56 adjacent amphibole and plagioclase rims at microcrack margins were determined by electron microprobe analysis. Operating conditions were: 15 kV accelerating potential, 8 nA beam current, and 20 s counting times. A ZAF correction algorithm was used with well characterized natural and synthetic standards. Compositional data are given in Table 1. Amphibole formulae and Fe^{3+} contents were calcu-

lated based on 23 anhydrous oxygens following Holland and Blundy [9]. Although normalization based on $\text{Si} + \text{Ti} + \text{Al} + \text{Fe} + \text{Mn} + \text{Mg} = 13$ may yield a more accurate approximation of Fe^{3+} content and site distribution [18], we used the anion-based recalculation to ensure consistency with the thermometer calibration.

Amphibole compositions are calcic (Fig. 2C), with a range in tetrahedrally coordinated Al ($^{\text{IV}}\text{Al}$) of 0.41–1.70. They are Mg rich, but Mg does not vary systematically with $^{\text{IV}}\text{Al}$ (Fig. 2A). Both Na + K in the A site and Na in the M4 site increase with $^{\text{IV}}\text{Al}$ (Fig. 2B,C), as is typical of high grade amphiboles from oceanic gabbros [8,19,20]. The ranges in $^{\text{IV}}\text{Al}$, and A- and M4-site occupancies arise from a dependence of amphibole composition on adjoining mineral identity: lower values occur where amphibole fills microcracks between pyroxenes and plagioclase, and higher values where the microfractures are bounded only by plagioclase [14]. The average X_{An}

Table 1
Representative amphibole analyses

Sample:	4R-01-9	4R-02-7	8R-01-10	8R-01-10	9R-04-11	9R-04-11	12R-03-3	13R-01-11B	17R-01-13	17R-01-1B
Depth (m):	45.9	48.2	71.1	71.1	78.7	78.7	98.1	105.2	127.8	128.6
Analysis:	a6	a50	16a2	20a3	a20	a24	13	59a4	18	a8
SiO_2	46.25	43.93	47.73	48.84	43.98	52.97	51.36	50.99	51.40	50.65
TiO_2	0.13	0.56	0.82	0.50	0.27	0.32	0.39	0.50	0.15	0.33
Al_2O_3	9.15	10.46	6.74	6.88	12.66	3.71	5.04	4.61	4.05	5.08
FeO	15.37	17.69	15.91	15.39	11.79	9.70	12.54	15.09	16.15	12.32
MnO	0.28	0.19	0.24	0.21	0.27	0.21	0.23	0.30	0.26	0.18
MgO	11.88	10.20	12.11	12.09	14.43	19.18	15.80	13.68	13.80	15.02
CaO	11.45	11.80	11.44	11.79	10.95	10.21	11.39	11.56	10.77	11.94
Na_2O	1.64	1.97	1.31	1.14	2.56	0.65	0.78	0.56	0.62	0.84
K_2O	0.06	0.20	0.18	0.15	0.12	0.02	0.09	0.10	0.00	0.11
Total	96.21	97.00	96.49	96.98	97.03	96.97	97.62	97.39	97.20	96.47
<i>Cations per 23 anhydrous oxygens</i>										
Si	6.855	6.575	7.072	7.177	6.347	7.494	7.350	7.425	7.503	7.344
$^{\text{IV}}\text{Al}$	1.145	1.425	0.928	0.823	1.653	0.506	0.650	0.575	0.497	0.656
$^{\text{VI}}\text{Al}$	0.453	0.421	0.249	0.367	0.501	0.113	0.200	0.216	0.199	0.212
Ti	0.014	0.063	0.091	0.055	0.030	0.034	0.042	0.055	0.017	0.036
Fe^{3+}	0.483	0.480	0.407	0.308	0.785	0.289	0.316	0.232	0.257	0.385
Mg	2.624	2.275	2.675	2.648	3.105	4.043	3.370	2.970	3.004	3.247
Fe^{2+}	1.422	1.733	1.564	1.584	0.638	0.859	1.185	1.606	1.715	1.108
Mn	0.036	0.024	0.029	0.026	0.032	0.026	0.028	0.037	0.033	0.022
Na	1.818	1.892	1.816	1.855	1.693	1.547	1.746	1.804	1.684	1.856
Ca	0.470	0.573	0.377	0.325	0.715	0.177	0.217	0.157	0.177	0.325
K	0.011	0.039	0.034	0.028	0.019	0.004	0.017	0.019	0.001	0.020
Total	15.331	15.501	15.244	15.196	15.518	15.093	15.122	15.095	15.085	15.212
X_{An}	0.802	0.479	0.476	0.449	0.708	0.615	0.566	0.553	0.354	0.688
T ($^{\circ}\text{C}$)	734	712	729	654	801	737	710	667	633	738

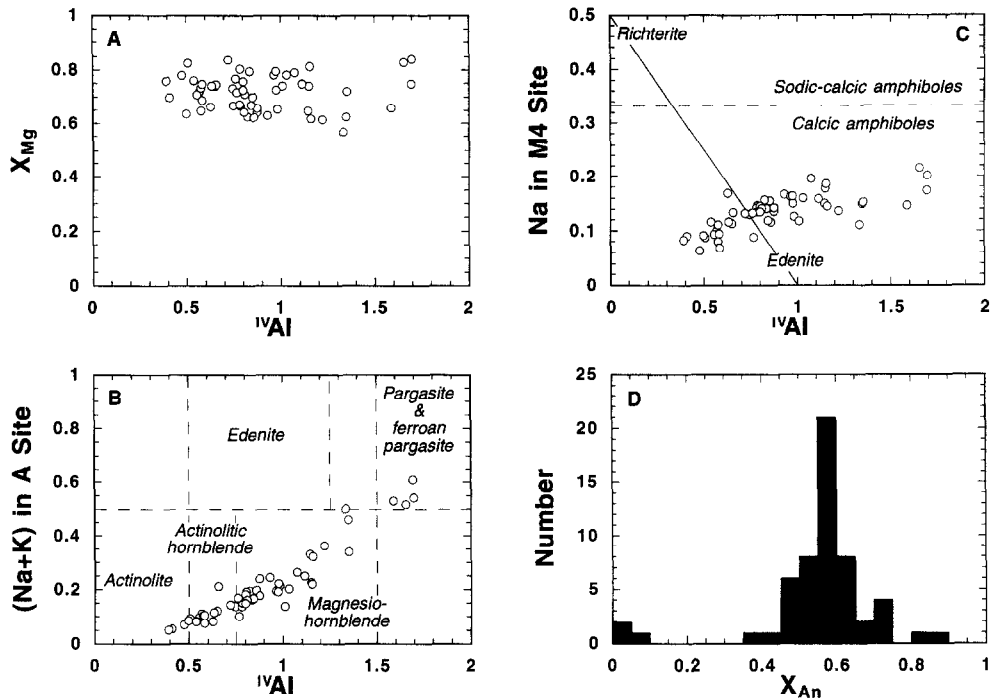


Fig. 2. Amphibole and plagioclase compositional parameters in pegmatitic and nonpegmatitic gabbros. Amphibole formulae based on 23 anhydrous oxygens after [9]; plagioclase formulae assume 8 oxygens and all Fe as Fe^{3+} . Relevant amphibole nomenclature after [35]. (A) Mole fraction of Mg ($X_{Mg} = Mg/(Mg + Fe^{2+})$) vs. tetrahedrally coordinated Al (^{IV}Al) in amphiboles. (B) Alkali cations in A site vs. ^{IV}Al in amphiboles. (C) Na in M4 vs. ^{IV}Al in amphiboles with richterite–edenite exchange trajectory used in temperature determination. Near-linear increase in M4 Na indicates that extent of richterite–edenite exchange is similar for all amphiboles, consistent with narrow calculated temperature interval. (D) Histogram of plagioclase compositions in terms of mole fraction of anorthite ($X_{An} = Ca/(Ca + Na)$).

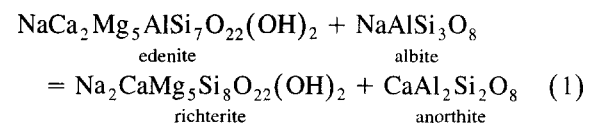
of coexisting plagioclase is 0.55 (Fig. 2D). Magmatic [13] and metamorphic plagioclase compositions overlap in terms of X_{An} , but secondary plagioclase is more tightly distributed about the mean, whereas magmatic plagioclase extends to high X_{An} .

Typical criteria used to establish textural, and by implication, chemical equilibrium are absent in Hess Deep gabbros because they are not strongly deformed and they show little grain-size modification associated with recrystallization. We nevertheless interpret the amphibole–plagioclase pairs as representing local equilibrium for three reasons. First, the plagioclase shows clear textural and compositional evidence for reaction with hydrothermal fluid in the microfracture network (Fig. 1). In addition, variations in compositions of vein-filling amphibole show systematic variation, which depends on local, compositionally distinct chemical environments [14], suggesting equilibration on the scale of several millimeters. Finally, $\delta^{18}O$ of plagioclase and amphibole

are lower than magmatic values, indicating equilibration with sea water [21]. Together, these observations suggest that the variable extent of metamorphism of Hess Deep gabbros was limited by low, locally variable water–rock ratios rather than approach to equilibrium. Similar conclusions have been drawn for other oceanic and continental gabbros [20,22].

4. Metamorphic temperatures

In the absence of quartz, the temperature of amphibole–plagioclase equilibration may be assessed through the extent of $[NaSi]_{-1}[CaAl]$ exchange among phase components [9,23]:



Holland and Blundy [9] used nonlinear least-squares regression and a well constrained plagioclase

solid-solution model to derive within-site and cross-site interaction parameters for amphibole solid-solution parameters. This allows calculation of temperature for appropriate compositions of plagioclase and amphibole.

Four of 56 pairs failed two compositional criteria imposed by Holland and Blundy's data set ($0.9 > X_{An} > 0.1$ or ${}^{IV}Al > 0.3$). Calculated temperatures for the remaining 52 compositionally appropriate amphibole–plagioclase pairs yield a mean of 716°C with one standard deviation (σ) of 36°C (Fig. 3). The observed standard deviation is similar to the value of 39°C for temperature residuals in the calibrant data set [9]. Skewness and kurtosis are -0.05 and 3.0 , virtually identical to a normal distribution. The standard error of the mean is 5°C, so the data constrain the distribution mean to be between 707° and 724°C at the 90% confidence level.

The accuracy of our calculated temperatures is difficult to assess. The thermometer is weighted strongly by experimental results, for which temperature is independently known with comparatively good accuracy, and Holland and Blundy [9] show that there are no systematic errors introduced by their formula normalization scheme. The most important accuracy issue is therefore the possibility of systematic differences in the compositions of the Hess Deep amphiboles and those of the calibrant data set. Because Holland and Blundy [9] ignored contributions to the energetics of mixing from Mn and Ti, from Fe and Mg on M4, and from F and Cl substitution, differences in the abundance of these elements could

cause errors in calculated temperatures. As shown in Table 1, Mn and Ti contents of Hess Deep amphiboles are uniformly low, so potential errors attributable to these cations are probably minimal. In addition, the mean cummingtonite component of the data set is 0.075 and inferred temperatures show no dependence on the extent of calculated M4 occupancy by cations other than Ca and Na. Three amphiboles had cummingtonite component > 0.2 and yield temperatures of 633–737°C, which implies that there are no systematic errors introduced by high cummingtonite content. We have not analyzed for F and Cl systematically, but Gillis [16] found that the concentrations of these anions is low (< 0.30 wt%). Thus, it appears that the compositional range in the Hess Deep amphiboles is unlikely to result in systematic errors.

The precision of any given temperature determination is constrained by the random errors in the thermometer, which are probably dominated by the amphibole recalculation scheme. In the absence of any apparent formula-dependent systematic errors in calculated temperature, it can be assumed that all errors associated with normalization are random and are reflected in the distribution of the differences between calculated and observed temperatures in the calibrant data set. An important source of random error may be the strong dependence of calculated temperature on Na distribution between A and M4 sites, which is estimated imprecisely by normalization based on 23 anhydrous oxygens [18].

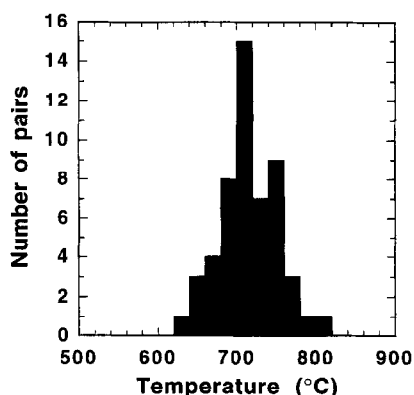


Fig. 3. Histogram of calculated temperatures from amphibole–plagioclase pairs.

5. Statistical approach to metamorphic rates in the oceanic lower crust

The distribution in Fig. 3 suggests that the mean temperature of earliest metamorphism of Hole 894G gabbros is high (716°C) and is constrained to lie in a narrow range ($\pm 8^\circ\text{C}$, 90% confidence interval). However, it is not the average temperature that is useful for constraining metamorphic thermal history, but rather the possible range of temperatures (ΔT) over which metamorphism occurred. Although the observed temperature distribution indicates that a single, instantaneous metamorphic event is possible between 707° and 724°C, such an event requires

fracturing, fracture filling by hydrothermal fluid, mineral–fluid reaction, and equilibration on an extremely short time scale. This may have taken place, but other metamorphic scenarios are also plausible. For example, the core may have fractured at slightly different temperatures at different locations, or a single fracture event may have affected the entire core, but the temperature of equilibration may not have been uniform. Our ability to distinguish between such scenarios is limited by the uncertainty in individual temperature determinations inherent in the thermometer calibration. Determination of the maximum ΔT therefore requires goodness-of-fit comparisons between observed and synthetic distributions, where synthetic distributions are generated by the convolution of plausible hypothetical thermal histories with the measurement uncertainty of the hornblende–plagioclase thermometer.

Comparison of synthetic and observed distributions first requires identification of plausible hypothetical thermal histories. If metamorphism was not instantaneous, it could have occurred in discrete events ranging from two to an infinite number of events separated infinitesimally in temperature. Thus, two reasonable end-member scenarios which should be considered are metamorphism in two discrete, instantaneous equilibration events (double distribution), for which ΔT is the absolute separation of events, and continuous metamorphism producing a uniform range of equilibration over some temperature interval (uniform distribution), with ΔT reflecting the entire temperature range. Equilibration events between these two end-members would produce intermediate temperature distributions, and thus provide no better constraint on the maximum ΔT . It is also possible that a large fraction of equilibration occurred at the time of initial fracturing, but equilibration continued to a diminishing extent as temperatures declined. This can be approximated as a distribution in which the number of observations declines exponentially from an initial temperature. Here, we take ΔT to be the range extending from the maximum down to the value at which 95% of the temperatures are included. We did not consider the converse scenario, in which the number of observations increases exponentially to a maximum at a temperature below which no further equilibration occurs, because it is geologically implausible. Finally, meta-

morphism may have resulted in equilibration temperatures normally distributed about a mean. In this case, ΔT was taken to be the range in values centered on the mean which includes 95% of the distribution.

Plausible hypothetical thermal histories with means of 716°C can be combined with the thermometer uncertainty to give synthetic measured temperature distributions, which can then be compared to the observed data to identify the goodness-of-fit test which most restricts the range of synthetic distributions consistent with the observed data. Potential tests include an F test on the ratio of variances [24], χ^2 tests on the variance and distribution [25,26], a modified Kolmogorov–Smirnov two-sample test [26], and kurtosis and skewness tests [26]. For the sample size and variance, it should be expected that the variances of the synthetic and observed distributions will provide the tightest constraints on the temperature range of gabbro metamorphism. The variance in the synthetic distributions (σ_s^2) is the convolution of the variance in the thermometer (σ_T^2) and the variance in the hypothetical thermal history (σ_H^2), which for independent distributions is simply:

$$\sigma_s^2 = \sigma_T^2 + \sigma_H^2 \quad (2)$$

(e.g., [27]). The thermometer error is assumed to be normally distributed with a mean of zero and a standard deviation of 39°C [9]. The variance for plausible hypothetical temperature distributions is a simple function of ΔT and the form of the distribution chosen. Eq. (2) can thus be written for the different scenarios as:

$$\text{Double: } \sigma_s^2 = 1521 + \Delta T^2/4 \quad (3A)$$

$$\text{Exponential: } \sigma_s^2 = 1521 + \Delta T^2/9 \quad (3B)$$

$$\text{Uniform: } \sigma_s^2 = 1521 + \Delta T^2/12 \quad (3C)$$

$$\text{Normal: } \sigma_s^2 = 1521 + \Delta T^2/16 \quad (3D)$$

[24,25]. For the distribution tests, we developed a simple Monte Carlo model that simulates 10,000 measured metamorphic temperatures by convolving the hypothetical temperature distributions with the normally distributed random thermometer error. Large Monte Carlo data sets were generated to enhance accuracy while avoiding tedious numerical integration (e.g., [25]). Comparison of these data sets

with the observed temperature distribution confirms that the variance tests are most restrictive. This is because 52 measurements constrain skewness and kurtosis poorly, and the Kolmogorov–Smirnov and χ^2 tests on the distribution are more sensitive to the middle parts of the distributions, whereas diagnostic differences appear to be in the tails.

The variance tests allow identification of the variance or standard deviation below which, at a given level of confidence, the synthetic and observed distributions cannot be distinguished, and hence the maximum ΔT of metamorphism consistent with the observed data set (Eq. (3A) Eq. (3B) Eq. (3C) Eq. (3D)). Fig. 4A illustrates the change in the standard deviation of synthetic temperature distributions with ΔT . At a given ΔT , the standard deviations of the synthetic temperature distributions increase from normal, through uniform and exponential, to double distributions because of the decreasing magnitude of the denominators in the right-hand terms in Eq. (3A) Eq. (3B) Eq. (3C) Eq. (3D). Clearly, for a given standard deviation, normally distributed metamorphic temperatures require the largest ΔT for the scenarios investigated. Adopting a confidence level of 90% to ensure a conservative result, the synthetic and observed distributions are indistinguishable below $\sigma_s = 41.8$ using both χ^2 and F tests. Fig. 4A illustrates that the corresponding maximum range in metamorphic temperature is 60°C. Thus, a conservative estimate of the range in metamorphic temperatures represented by our analyses is 686–746°C at the 90% confidence level.

6. Discussion

Combining our result with two-dimensional simulations of deformation and heat transport in the near-ridge environment of fast-spreading centers [28,29] allows prediction of the location and timing of gabbro metamorphism in Hole 894G. The models account for the effects of hydrothermal cooling and assume magma-lens geometry, consistent with recent studies of EPR magma chambers [30]. Fig. 4B shows that gabbros of fast-spreading environments cool through the amphibolite facies within several kilometers of the axis and less than 100,000 yr after emplacement. Differences in the cooling paths arise

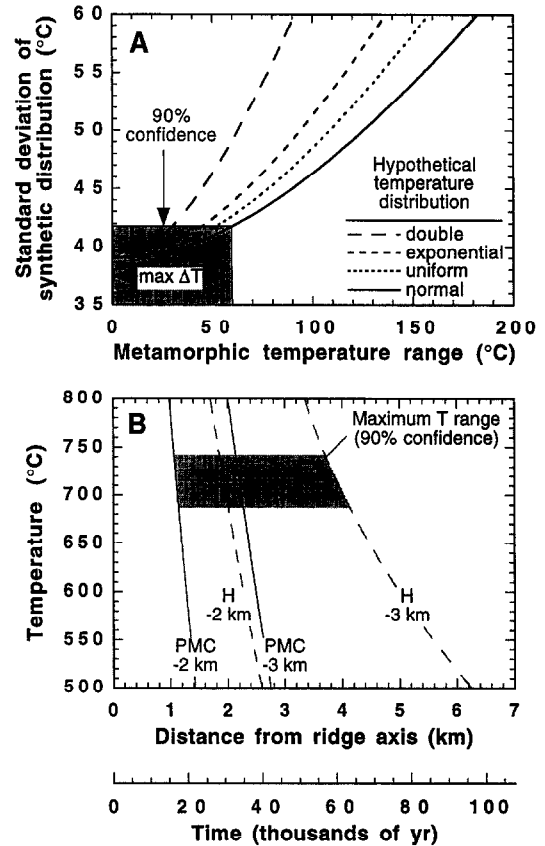


Fig. 4. (A) Variation in standard deviation of simulated distributions with temperature range (ΔT) of the hypothetical events (see text). At the 90% confidence level, the simulated distributions cannot be distinguished from the observed distribution (Fig. 2) when $\sigma \leq 41.8$, which corresponds to a different ΔT for each hypothetical thermal history. The maximum (most conservative) ΔT at the 90% confidence interval is 60°C, which would have occurred if the observed distribution was produced by normally distributed underlying temperatures. The shaded box contains all ΔT and standard deviations of the hypothetical thermal histories that are consistent with the observed distribution. (B) Temperature vs. distance from ridge axis as predicted for 2 and 3 km depth from simulations by Phipps Morgan and Chen [28] (PMC) and Henstock et al. [29] (H). Spreading rates were transformed from 50 and 55 mm/yr to 65 mm/yr; in [29], the model using a 1 km wide sill was used (see their fig. 7A). The shaded region denotes the maximum ΔT of 60°C about the mean of 716°C. Metamorphic durations are derived by subtracting time at which 746°C isotherm is crossed from the time of cooling to 686°C for a given depth.

from the different extents of hydrothermal cooling and slightly different magma lens geometry in the models of Phipps Morgan and Chen [28] and Henstock et al. [29], as well as from depth in the crust. In

both models, cooling of gabbros at 2–3 km below sea floor is dominated by conduction, which is consistent with the low fluxes inferred from amphibole compositions [14] and O and Sr isotopic results [21].

Because the stratigraphic position of the gabbros is not well constrained, Hess Deep gabbros could have been metamorphosed anywhere from 1 to 4 km off the EPR, 15,000 to 64,000 yr after axial emplacement. However, despite the somewhat wide range in possible position and timing of metamorphism, our result requires that the duration of metamorphism was short. Fig. 4B shows that gabbros at 2 km depth in the model of Henstock et al. cool through 746–686°C between 24,600 and 26,300 yr after axial emplacement, or in 1700 yr; gabbros at 3 km depth require 5800 yr for the same decrease in temperature. In Phipps Morgan and Chen's model, metamorphic duration is 1000–1600 yr at the same depths (Fig. 4B). By contrast, the time required to cool from 800°C to 500°C is 12,200–38,000 yr [29] or 5400–9000 yr [28]. Thus, whatever the stratigraphic position of the Hole 894G gabbros within the 2–3 km depth interval, the metamorphic event occurred over several thousand years at most, or a factor of 5–7 more quickly than would be predicted from the broader temperature range of 500–800°C.

Our interpretation of rapid early metamorphism over no more than ~6000 yr is conservative for three reasons. First, we use the maximum ΔT permissible at a high confidence level (Fig. 4A); decreasing confidence level to 75–80%, or decreasing ΔT to 20–40°C (consistent with any of the other model temperature distributions) would lead to metamorphic duration of hundreds of years in all scenarios except the greatest depths in the models of Henstock et al. [29]. Second, local reequilibration of individual amphibole–plagioclase pairs during cooling may contribute to the range of temperatures we computed; if this could be accounted for, the inferred duration of the metamorphic event would decrease. And finally, the simulations ignore along-strike variability in magma chamber and axial geometry [31] that cause variations in hydrothermal flow and thermal structure along the EPR [32]. Such variations may lead to more rapid cooling nearer the axis and could decrease our inferred duration of metamorphism if faulting related to axial discontinuities enhanced advective heat transport at depth, although,

as noted above, Hole 894G gabbros show no evidence for this.

The inferred maximum temperature range for early metamorphism of 686–746°C at the 90% confidence level is petrologic support for the hypothesis that the seismic brittle–ductile transition is 700–800°C [28,33,34], independent of spreading rate. Maximum depths of earthquake foci in oceanic lithosphere decrease with increasing spreading rate and correlate well with the predicted 750°C isotherm for varying spreading rates when hydrothermal cooling is taken into account [28]. Given that brittle failure, such as the microfracture network in Hole 894G gabbros, can only occur below the brittle–ductile transition, the temperatures required by the minerals filling the microfractures place a lower limit on its temperature.

Temperature constraints on microscopic amphibole veins in Hess Deep gabbros from ODP Hole 894G argue for the initiation of fracturing, fluid flow, and fluid–rock reaction between 746°C and 686°C during a short-lived event lasting no more than several thousand years. The high temperatures of metamorphism imply the onset of brittle failure at temperatures near the inferred seismic brittle–ductile transition. If our result is typical for EPR gabbros, it raises the possibility that metamorphism of the lower crust in fast-spreading centers may occur rapidly, sporadically, and locally, rather than homogeneously throughout the crust.

Acknowledgements

Supported by JOI-USSAC USSSP035/147-20720b. Comments by E. Essene and an anonymous reviewer substantially improved the manuscript. We thank C. MacLeod, A. Yin, and M. Grove for comments and discussion of early versions of this work. C. Bacon and L. Calk kindly made the electron microprobe facility, U.S.G.S, Menlo Park, available to us at an early stage of this project. [C/L]

References

- [1] C. Mével and M. Cannat, Lithospheric stretching and hydrothermal processes in oceanic gabbros from slow-spreading ridges, in: *Ophiolite Genesis and Evolution of the Oceanic Lithosphere*, T. Peters, A. Nicolas, and R.G. Coleman, eds., pp. 293–312, Kluwer, Dordrecht, The Netherlands, 1991.

- [2] K.M. Gillis, Controls on hydrothermal alteration in a section of fast-spreading oceanic crust, *Earth Planet. Sci. Lett.* 134, 473–489, 1995.
- [3] J.G. Liou, S. Kuniyoshi and K. Ito, Experimental studies of the phase relations between greenschist and amphibolite in a basaltic system, *Am. J. Sci.* 274, 613–632, 1974.
- [4] F.S. Spear, An experimental study of hornblende stability and compositional variability in amphibolite, *Am. J. Sci.* 281, 697–734, 1981.
- [5] D.J. Anderson, D.H. Lindsley and P.M. Davidson, QUILF: a PASCAL program to assess equilibria among Fe–Mg–Mn–Ti oxides, pyroxenes, olivine and quartz, *Comput. Geosci.* 19, 1333–1350, 1993.
- [6] H. Helmstaedt and J.M. Allen, Metagabbro from DSDP Hole 334: an example of high temperature deformation and recrystallization near the Mid-Atlantic Ridge, *Can. J. Earth Sci.* 14, 886–898, 1977.
- [7] C.E. Manning and D.K. Bird, Hydrothermal clinopyroxenes of the Skaergaard intrusion, *Contrib. Mineral. Petrol.* 92, 437–447, 1986.
- [8] K.M. Gillis, G. Thompson and D.S. Kelley, A view of the lower crustal component of hydrothermal systems at the Mid-Atlantic Ridge, *J. Geophys. Res.* 98, 19,597–19,619, 1993.
- [9] T.J.B. Holland and J.D. Blundy, Non-ideal interactions in calcic amphiboles and their bearing on amphibole–plagioclase thermometry, *Contrib. Mineral. Petrol.* 116, 433–447, 1994.
- [10] P. Lonsdale, Structural pattern of the Galapagos Microplate and evolution of the Galapagos triple junctions, *J. Geophys. Res.* 93, 13,551–13,574, 1988.
- [11] J. Francheteau, R. Armijo, J.L. Cheminée, R. Hekinian, P. Lonsdale and N. Blum, 1 Ma East Pacific Rise oceanic crust and uppermost mantle exposed by rifting in Hess Deep (equatorial Pacific Ocean), *Earth Planet. Sci. Lett.* 101, 281–295, 1990.
- [12] K.M. Gillis, C. Mével, J. Allan and the Leg 147 Scientific Party, *Proc. ODP Init. Rept.* 147, 1993.
- [13] J.H. Natlund and H.J.B. Dick, Melt migration through high-level gabbroic cumulates of the East Pacific Rise at Hess Deep: inferences from rock textures and mineral compositions, *Proc. ODP Sci. Results* 147, 21–58, 1996.
- [14] C.E. Manning and C.J. MacLeod, Fracture-controlled metamorphism of Hess Deep Gabbros, Site 894: constraints on the roots of mid-ocean ridge hydrothermal systems at fast spreading centers, *Proc. ODP Sci. Results* 147, 189–212, 1996.
- [15] R.B. Pederson, J. Malpas and T. Falloon, Petrology and geochemistry of gabbroic and related rocks from Site 894, Hess Deep, *Proc. ODP Sci. Results* 147, 3–19, 1996.
- [16] K.M. Gillis, Trace element constraints on the origin of amphibole in gabbroic rocks from ODP Site 894, Hess Deep, *Proc. ODP Sci. Results* 147, 59–75, 1996.
- [17] P.E. Weston and C.E. Manning, High temperature fracturing at Hess Deep: implications for initiation of lower crustal brittle deformation at the East Pacific Rise, *Eos* 76 (Suppl.), F709, 1995.
- [18] M.A. Cosca, E.J. Essene and J.R. Bowman, Complete chemical analyses of metamorphic hornblendes: implications for normalizations, calculated H₂O activities, and thermobarometry, *Contrib. Mineral. Petrol.* 108, 472–484, 1991.
- [19] D.S. Stakes, C. Mével, M. Cannat and T. Chaput, Metamorphic stratigraphy of Hole 735B, *Proc. ODP Sci. Results* 118, 153–180, 1991.
- [20] D.S. Stakes and D.A. Vanko, Multistage hydrothermal alteration of gabbroic rocks from the failed Mathematician Ridge, *Earth Planet. Sci. Lett.* 79, 75–92, 1986.
- [21] C. Lécuyer and G. Gruau, Oxygen and strontium isotope compositions of Hess Deep gabbros (Holes 894F and G): high-temperature interaction of seawater with the oceanic crust layer 3, *Proc. ODP Sci. Results* 147, 227–234, 1996.
- [22] D.K. Bird, R.D. Rogers and C.E. Manning, Mineralized fracture systems of the Skaergaard intrusion, East Greenland, *Meddel. Grønland Geosi.* 16, 1–68, 1986.
- [23] F.S. Spear, NaSi ⇌ CaAl exchange equilibrium between plagioclase and amphibole: an empirical model, *Contrib. Mineral. Petrol.* 72, 33–41, 1980.
- [24] M.R. Spiegel, *Theory and Problems of Probability and Statistics*, 372 pp., McGraw-Hill, New York, 1975.
- [25] P.R. Bevington and D.K. Robinson, *Data Reduction and Error Analysis for the Physical Sciences*, 328 pp., McGraw-Hill, New York, 1992.
- [26] W.H. Press, S.A. Teukolsky, W.T. Vetterling and B.P. Flannery, *Numerical Recipes in C*, 994 pp., Cambridge University Press, Cambridge, 1992.
- [27] A. Papoulis, *Probability, Random Variables, and Stochastic Processes*, 583 pp., McGraw-Hill, New York, 1965.
- [28] J. Phipps Morgan and Y.J. Chen, The genesis of oceanic crust: magma injection, hydrothermal circulation, and crustal flow, *J. Geophys. Res.* 98, 6283–6297, 1993.
- [29] T.J. Henstock, A.W. Woods and R.S. White, The accretion of oceanic crust by episodic sill intrusion, *J. Geophys. Res.* 98, 4143–4161, 1993.
- [30] J.M. Sinton and R.S. Detrick, Mid-ocean ridge magma chambers, *J. Geophys. Res.* 97, 197–216, 1992.
- [31] K.C. Macdonald, D.S. Scheirer and S.M. Carbotte, Mid-ocean ridges: discontinuities, segments and giant cracks, *Science* 253, 986–994, 1991.
- [32] R.M. Haymon, D.J. Fornari, M. Edwards, S.M. Carbotte, D. Wright and K.C. Macdonald, Hydrothermal vent distribution along the East Pacific Rise crest (9°09′–54′N) and its relationship to magmatic and tectonic processes on fast spreading mid-ocean ridges, *Earth Planet. Sci. Lett.* 104, 513–534, 1991.
- [33] D.A. Wiens and S. Stein, Intraplate seismicity and stresses in young oceanic lithosphere, *J. Geophys. Res.* 88, 6455–6468, 1983.
- [34] E.A. Bergman and S.C. Solomon, Source mechanisms of earthquakes near mid-ocean ridges from body waveform inversion: implications for the early evolution of oceanic lithosphere, *J. Geophys. Res.* 89, 11,415–11,441, 1984.
- [35] B.E. Leake, Nomenclature of amphiboles, *Can. Mineral.* 16, 501–520, 1978.